Enabling Seamless Wireless Power Delivery in Dynamic Environments

This paper reviews magnetically coupled resonance techniques with related challenges, and discusses various methods used to adapt to the variations in range, orientation, and load, using both wideband and fixed-frequency techniques, in particular.

By Alanson P. Sample, *Member IEEE*, Benjamin H. Waters, *Student Member IEEE*, Scott T. Wisdom, *Student Member IEEE*, and Joshua R. Smith, *Senior Member IEEE*

ABSTRACT | Effective means of delivering wireless power to volumes of spaces will enable users the freedom and mobility to seamlessly power and recharge their devices in an unencumbered fashion. This has particular importance for consumer electronic, medical, and industrial applications, where usage models focus on unstructured and dynamic environments. However, existing wireless power technology falls short of this vision. Inductive charging solutions are limited to near-contact distances and require a docking station or precise placement for effective operation. Far-field wireless power techniques allow much greater range, but require complicated tracking systems to maintain a line-of-sight connection for high-efficiency power delivery to mobile applications. Recent work using magnetically coupled resonators (MCRs) for wireless power delivery has shown a promising intersection between range (on the order of a meter), efficiency (over 80%), and delivered power (up to tens of watts). However, unpredictable loads rapidly change system operating points, and changes in position disrupt system efficiency, which affects the ultimate usability of these systems. Dynamic adaptation to these changes in operating conditions and power transfer range is a critical capability in developing a fully functional and versatile wireless power solution. This paper provides an overview of methods used to adapt to variations in range, orientation, and load using both wideband and fixed-frequency techniques.

I. INTRODUCTION

Wireless power transfer using inductive coupling is becoming increasingly popular for consumer electronic devices. Commercial applications include wireless charging pads, electronic toothbrushes, induction cookers, and electric vehicle recharging. However, none of these applications enable the geometric freedom that the term wireless power suggests. Inductive charging pads and electric toothbrushes require that the device be placed very close to (or directly on top of) the charging pad. This is due to the fact that the efficiency for traditional inductively coupled wireless power transfer systems drops off rapidly as the distance between the transmitter and the receiver increases [1], [2].

Far-field wireless power transfer techniques use propagating electromagnetic waves and are capable of delivering power to much larger volumes of space. However,

there is an inherent tradeoff between directionality and transfer efficiency. For instance, radio-frequency (RF) broadcast methods, which transmit power in an omnidirectional pattern, allow for power transfer anywhere in the coverage area. In this case, mobility is maintained, but end-to-end efficiency is lost since power density decreases with a $1/r^2$ dependency [3]. On the other hand, microwave systems with high-gain antennas have been used to transfer power over several kilometers at efficiencies of over 90% [4], [5]. However, these systems suffer from the need for sophisticated tracking and alignment equipment to maintain a line-of-sight (point-to-point) connection in unstructured and dynamic environments.

Furthermore, regulatory restrictions limit the amount of power that can be transmitted in uncontrolled environments for safety as well as for emissions and interference reasons. As a result, the main commercial use of far-field wireless power transfer is for passive (i.e., battery free) ultrahigh-frequency (UHF) radio-frequency identification (RFID) tags, which are limited to 4-W equivalent isotropic radiated power (EIRP) in the United States [6].

Recent research efforts using magnetically coupled resonators (MCRs) for wireless power transfer have demonstrated the potential to deliver power with more efficiency than far-field broadcast approaches, and at longer ranges than traditional inductively coupled schemes [7]–[12]. These techniques use high-Q coupled resonators that transfer energy via magnetic fields (which do not strongly interact with the human body), and ongoing work has shown that more power can be safely transmitted via MCRs than traditional far-field techniques [13].

Applications include wirelessly recharged and powered consumer electronics electric vehicles and implanted medical devices. However, very few end-to-end systems can adapt to changes in the environment. Unpredictable loads and changes in distance and orientation rapidly change system operating points, which disrupt the end-to-end wireless

power transfer efficiency. Dynamic adaptation of a system to these types of events is a critical capability in developing fully functional and versatile wireless power solutions.

This paper provides a comprehensive overview of methods used to adapt to variations in range, orientation, and load, using both wideband and fixed-frequency techniques. In particular, we present a detailed comparison of: impedance matching techniques used for fixed-frequency operation, adaptive frequency tuning for wider bandwidth systems, and adaptive load-matching techniques utilizing maximum power point tracking (MPPT). Finally, we present a full end-to-end system capable of adapting to real-time changes in the environment while maintaining optimal efficiency. Our system demonstrates a robust means of wireless power delivery that takes advantage of the full volume of space available and accounts for changes in distance and alignment.

II. SYSTEM OVERVIEW

This work focuses on methods that take advantage of the unique properties of MCRs to enable seamless wireless power delivery to volumes of space. A detailed description of the operating principles and performance characteristics of MCRs is presented in [8]. This section will provide a brief overview of the system and highlight key features that can enable seamless wireless power delivery.

Fig. 1 shows a diagram of a basic wireless power system using MCRs. The transmitter module consists of a single-turn drive loop and a multiturn spiral resonator. When the RF amplifier drives current through the drive loop at the system's resonant frequency, the resulting oscillating magnetic field excites the Tx coil; the coil stores energy in the same manner as a discrete series LCR tank (consisting of an inductor, a capacitor, and a resistor). This results in a large oscillating magnetic field in the vicinity of the transmit coil. A high coil quality factor means that more energy
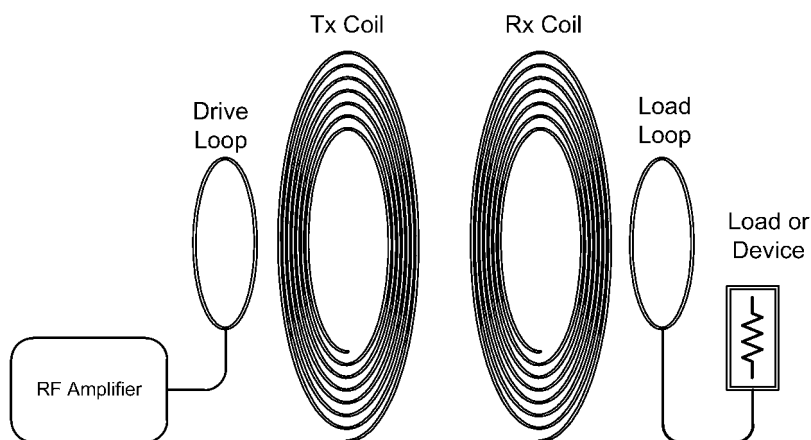

Fig. 1. *Sketch of the magnetically coupled resonant wireless power system consisting of an RF amplifier capable of controlling the magnitude and frequency of the transmitted signal. A two-element transmitter wirelessly powers the two receive resonators and the load device.*

can be stored on the coil, which also results in greater magnetic flux density at a given point in space.

The receiver module is designed similarly. It consists of a multiturn spiral resonator and a single-turn load loop, which is connected to the end device. Just as the loop and the coil are magnetically coupled, the transmit and receive coils share a mutual inductance, which is a function of the geometry of the coils and the distance between them. The key insight is that the high-Q transmit and receive coils form a single system of coupled resonators, which can easily transfer energy back and forth. It is important to note that the system coils do not radiate electromagnetic energy into free space. In fact, when the RF amplifier is driving the transmitter without a receiver present, all of the power not dissipated by the parasitic resistance of the coil is reflected back to the RF amplifier.

Fig. 2 shows the typical v-shaped plateau of efficiency versus distance and frequency for MCRs. This figure was generated by measuring the set of MCRs shown in Fig. 3 with a 50-Ω vector network analyzer. Frequency sweeps were taken at incremental distances along the common axis of the spiral coil, and the resulting S_{21} measurement was converted to efficiency ($\eta = |S_{21}|^2$). These reference coils will be used throughout this paper, and a detailed summary of their properties can be found in the Appendix.

Referring back to Fig. 2, the coupling coefficient between the Tx and Rx resonators is inversely proportional to the distance between them. As the separation distance increases, the amount of coupling between the resonators decreases, and the frequency separation of the two modes also decreases until the two resonant peaks converge at the fundamental frequency of the system. This convergence can be seen as the two ridges of the plateau merge at 13.56 MHz in Fig. 2.
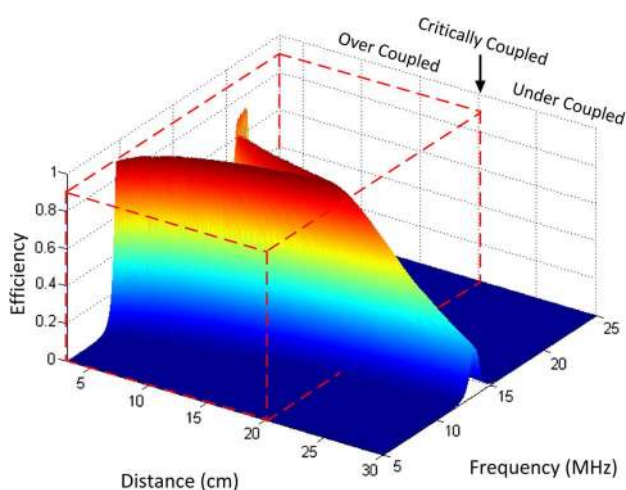
Fig. 3. *Image of the two high-Q MCRs used for wireless power transfer. These coils will be used as an experimental reference throughout this work and are referred to in the text as the "blue coils," since the insulation used to coat the wires is blue. The outer radius of the coils is 14 cm, and a detailed summary of their properties can be found in the Appendix.*

In this visualization, the overcoupled regime is represented by the area where frequency splitting occurs. In this regime, the resonators share more magnetic flux than is required to source the load. As will be shown in Sections III–V, proper tuning techniques will enable near-constant efficiency whenever the system operates in the overcoupled regime.

In the undercoupled regime, the shared flux falls below a critical point. Below this point, the power amplifier delivers more power to maintain the magnetic field than can be absorbed by the receiver. The result is that maximum efficiency cannot be achieved. Critical coupling is the point of transition between these two regimes and corresponds to the greatest range at which maximum efficiency can still be achieved. Similar to inductive coupling, the undercoupled regime is still capable of wireless power transfer, but efficiency decreases rapidly as distance increases.

This work aims to take advantage of the overcoupled regime to create volumes of space where a receiver and a load device can be wirelessly powered at maximum efficiency. It should be noted that Fig. 2 only represents a 1-D path as the receiver moves away from the transmitter. When operating, the transmit coil generates a large toroidal-shaped magnetic field that fills a large volume of space. Therefore, there are a wide variety of locations and orientation where the mutual inductance between the transmitter and the receiver will be sufficient to support the overcoupled regime.

Fig. 2. *Efficiency plateau of the MCR system as a function of the distance separation and frequency. The overcoupled regime represents the region where maximum power transfer can be achieved at near-constant efficiency if the system is properly tuned.*

III. ADAPTIVE FREQUENCY TUNING

Coupled oscillating systems have multiple modes of operation depending on the strength of the coupling between
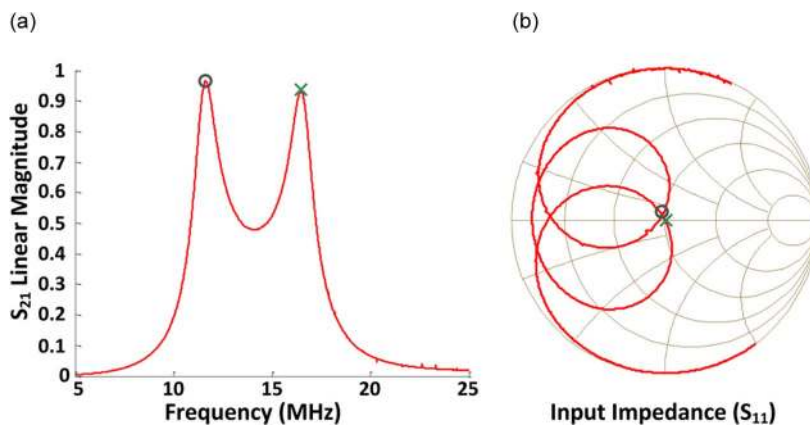
Fig. 4. *Measured scattering parameters for the blues coils at a distance of 7.8 cm along the axis of coil. Panel A shows the S_{21} linear magnitude of the system. Clearly visible are the two resonant modes caused by the coupling of the two high-Q resonators. Panel B shows the Smith chart of the input impedance (S_{11}) as the function of frequency. This panel shows that there are two frequencies where the input impedance to the coils is well matched to the 50-Ω source and maximum power transfer can occur.*

the resonators. This can be seen in the analogous case of two masses connected by a spring [14]. In this classic physics example, the two masses form a single system which can oscillate in two modes: one of higher frequency (even mode) and one of lower frequency (odd mode) than the fundamental frequency of an individual pendulum.

In the case of MCRs used in this work, the two modes of the system can be clearly seen in Fig. 4. Panel A shows the S_{21} linear magnitude, which is a measure of the transmission power gain across the system. This S_{21} plot represents a 2-D slice of the efficiency plateau plot in Fig. 2 at a separation distance of 7.8 cm. Notice that the two peaks indicate that the system is in the overcoupled regime. Panel B shows the input impedance (S_{11}) of the system on a Smith chart, which is normalized to 50 Ω. A black circle and a green cross approximately indicate where the peaks in the linear magnitude plot occur in the Smith chart. The ultimate goal is to ensure that an RF amplifier with characteristic impedance of 50 Ω can be well matched to the MCRs. These plots show that indeed the frequencies of peak $|S_{21}|$ correspond to a 50-Ω input impedance to the coils.

The goal of dynamic frequency tuning is to automatically adjust the transmitter frequency to provide maximum possible efficiency as a user moves the receiver to locations within the system's working range. This is accomplished by introducing a directional coupler between the amplifier and the drive loop. The coupler allows the transmit system to continuously measure the incident and reflected power as a function of frequency. Since this system forms a transmission line, the power not consumed by the load is reflected back to the source. By measuring the incident and reflected power using the directional coupler, the transmit system constantly adjusts the operating frequency such that the input impedance of the coils matches the impedance of the source coils. This results in optimal power transfer over the entire area of the overcoupled regime.

The mutual inductance between the transmitter and the receiver is a function of the coil geometry and the distance and/or orientation between them. Furthermore, the critical coupling point defines the transition from the overcoupled to undercoupled regime. The transformation from coupling space to distance can be difficult to visualize. Therefore, in order to characterize the area and the shape of space that can be wirelessly powered by MCRs, we examined the effect of both orientation and distance on power transfer efficiency.

Orientation has a significant effect on power transfer efficiency. A parallel configuration allows for the highest achievable coupling between the MCRs because a maximum amount of magnetic flux passes through the opening of the coils. On the other hand, the perpendicular case represents the worst case scenario for wireless power transfer efficiency because a minimal amount of magnetic flux passes through the receive coil. To demonstrate how efficiency varies between parallel and perpendicular orientations, actual measurements of efficiency were taken. The receive coil was held 14 cm away from the transmit coil and rotated in place by increments of 5°. The root mean square (RMS) received power was measured using an Agilent E4418B series power meter. Fig. 5 shows variations between 0° and 90° orientation versus power transfer efficiency both with and without adaptation. Fig. 5 shows that single-frequency operation without adaptation achieves lower efficiency for 0°–70° than the two cases with adaptation. Beyond that orientation, the efficiency drops off rapidly as the coils approach a 90° orientation.

To visualize the effect of distance between the coils, we measured the efficiency at each point on a 60 × 60-cm² grid. The first column of Fig. 6 shows a top view of the two experimental configurations. In panel 1A, the receive coil is parallel to the transmit coil. In panel 2A, the receive coil is perpendicular to the transmit coil. In both cases, the
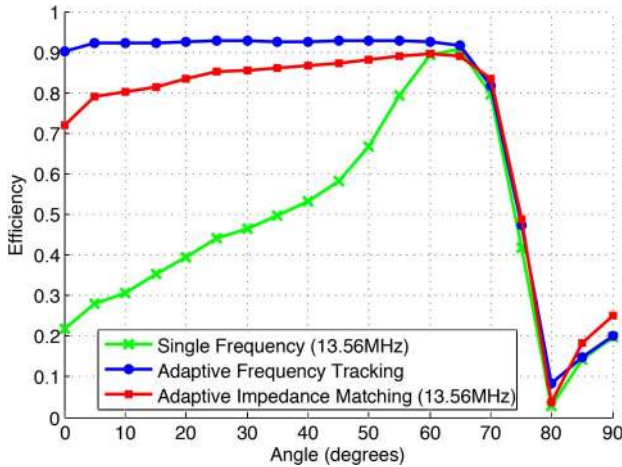
Fig. 5. *Measured efficiency of the blue coils at a distance of 14 cm between the transmit coil and the receive coil. The angle of misalignment between the transmit and receive coils is varied by 5° increments.*

transmit coil was held stationary at the origin of the grid, while the receive coil was moved in 3.7-cm increments along the X and Y dimension. For all experiments, the smart transmitter described in Section VI was used to transmit 5 W through the MCR systems both with and without adaptation, and the RMS received power was measured using an Agilent E4418B series power meter.

In the first experiment, the smart transmitter was used to transmit 5 W through the MCR systems at a fixed frequency tone of 13.56 MHz. From these results, the wireless power transfer efficiency is plotted in Fig. 6. The results for the parallel case can be seen in panel 1B as a donut-shaped ring of high-efficiency power transfer around the transmitter. Although this plot shows that it is possible to transfer wireless power without adaptive techniques, the area within 10 cm of the transmit coil indicates very low efficiency, which would not be acceptable for most wireless charging applications. The results for the perpendicular case can be seen in panel 2B of Fig. 6 as four peaks with a null when a perpendicular coil is positioned at the center of the opposite coil. The 28×28-cm^2 square at the center of panels 2B, 2C, and 2D represents the region that is physically impossible to measure because the coils cannot overlap.

In the second experiment, adaptive frequency tuning is enabled and the same experiment is repeated. Panel 1C in Fig. 6 shows a dramatic improvement in the serviceable area of the wireless power system. The experiment yielded a peak efficiency of 96.4% and a plateau of near-constant efficiency that covers a majority of the grid. Although panels 1B and 1C both show the characteristic toroidal shape of a magnetic field, frequency tuning can take advantage of the overcoupled regime to maximize the power transfer across the entire space. Panels 2B and 2C in Fig. 6 are nearly equivalent because the coupling coefficient
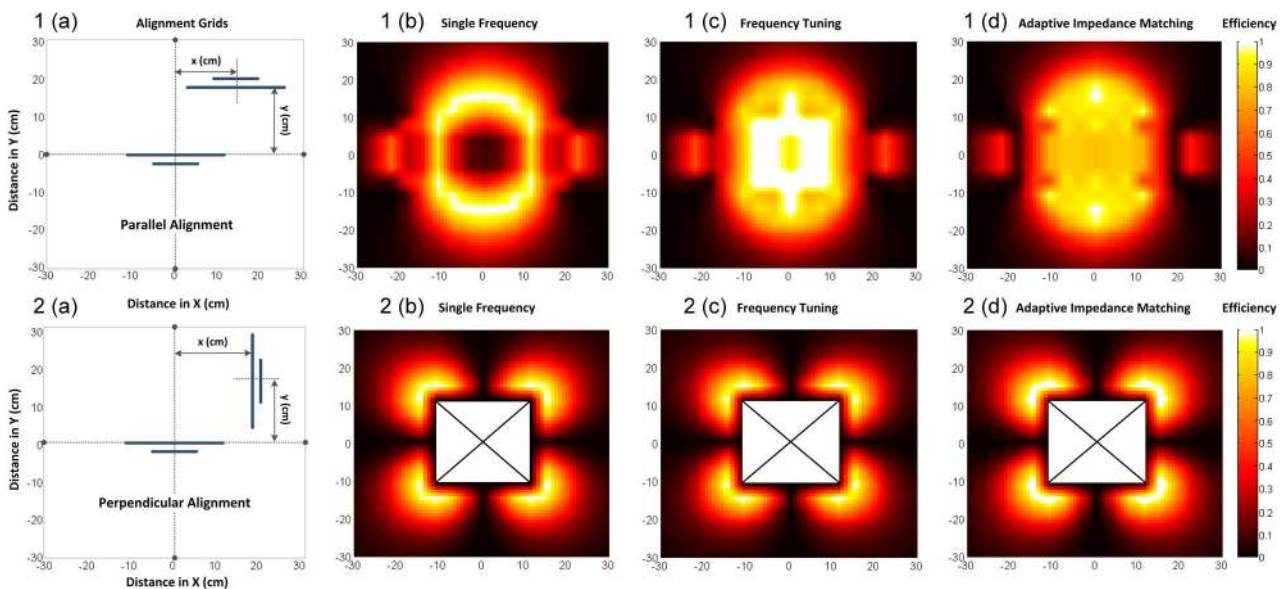
Fig. 6. *Wireless power transfer efficiency plots of MCRs with and without adaptation enabled for the cases when the transmit and receive coils are parallel (panel 1A) and perpendicular (panel 2A). Panels 1B and 2B show the regions of space that can be wirelessly powered at a fixed frequency with adaptation disabled. Panels 1C and 2C show dynamic frequency tracking enabled, which allows the system to take advantage of the overcoupled regime. Panels 1D and 2D show the use of adaptive impedance matching, which allows for single-frequency, narrowband operation. Panels 1C and 1D clearly show a high-efficiency plateau which allows for near-constant efficiency as a function of location, when adaptation is enabled. Panels 2B, 2C, and 2D show nearly equivalent efficiency for single-frequency operation, adaptive frequency tracking, and adaptive impedance matching.*

between the two coils never reaches the overcoupled regime for the perpendicular configuration. Thus, the optimal frequency that is selected for adaptive frequency tracking is almost always the same (13.56 MHz), which is the resonant frequency of each of the individual coils as measured in isolation.

IV. ADAPTIVE IMPEDANCE MATCHING

In Section III, wideband frequency tuning was used to achieve maximum efficiency in the overcoupled regime. In this section, dynamic impedance matching networks are used to maintain high efficiency at a single frequency. Narrow bandwidth operation is desirable for regulatory reasons.

A. Regulatory Compliance

Spectrum use regulations vary from country to country. Currently, no country has allocated spectrum specifically for wireless power transfer. However, the industrial–scientific–medical (ISM) bands are allocated internationally for RF applications other than communication. ISM bands are currently used for applications such as magnetic resonance imaging (MRI), RF heating, and microwave ovens. Therefore, they are a natural choice for wireless power transfer systems. Eventually, if wireless power transfer becomes widespread, one might imagine bands dedicated specifically for this purpose.

The ISM bands are currently governed in the United States by Parts 15 and 18 of the U.S. Federal Communication Commission (FCC) rules [6], [15]. Part 15 of the FCC rules covers intentional RF radiators and Part 18 covers specific ISM devices such as MRI and induction heaters. It may be desirable for wireless power systems to be covered by Part 18 because the radiated emission limits of Part 15 are more stringent than those of Part 18.

Regardless of how wireless power will integrate with governmental regulations on RF emissions, existing ISM bands are too narrow to accommodate frequency tuning. Consider the blue coils shown in Fig. 3, which are used throughout this paper. Fig. 2 shows that in order to maximize efficiency at any distance with these coils, it is necessary to tune from 8 to 22 MHz, a bandwidth of 14 MHz. However, the relevant ISM band is only 14 kHz wide, spanning 13.553–13.567 MHz. In this example, the bandwidth requirements of dynamic frequency tuning exceed the available bandwidth from FCC regulations by three orders of magnitude.

B. Consideration of Two-, Three-, or Four-Element Wireless Power Systems for Impedance Matching

An important question that any wireless power system designer must answer is how many coils to use. Prior work has analyzed the improvements in overall efficiency of two-, three-, and four-element systems using circuit theory, reflected load theory, and coupled mode theory [9], [16]–[18]. The common conclusion is that for two- and three-

element systems, at least one of the high-Q coils will be loaded down by the source resistance R_S from the power amplifier or the load impedance R_L of the RF rectifier/load application, which significantly reduces the Q of the resonator. Low Q limits the amount of energy that can be stored in the coils and thus reduces the magnetic flux density for a given location. The result is that the maximum range at which efficient wireless power transfer can be achieved is decreased [8]. Therefore, it is desirable to isolate the high-Q coils from the source and load impedances using a transformer or impedance matching network. The four-element system offers a unique advantage in this regard. Since the transmit loop and coil act as an air core step-up transformer and the receive loop and coil act as an air core step-down transformer, a wider range of tunable impedance transformation ratios is possible with a static four-element system compared to a static two- or three-element system. However, a combination of the two-, three-, or four-element systems with an adjustable impedance matching network can be the best approach for maximum range and efficiency while operating within a narrow frequency range.

In this section, we analyze the use of two-, three-, or four-element systems from an impedance matching perspective. Using the parasitic parameters of the coils in Table 2, the input impedance for a two-element system (coil–coil), a three-element system (loop–coil–coil), and a four-element system (loop–coil–coil–loop) can be calculated using

$$Z_{IN,2} = Z_1 + \frac{\omega^2 M_{12}^2}{Z_2} \tag{1}$$

$$Z_{IN,3} = Z_1 + \frac{\omega^2 M_{12}^2}{Z_2 + \dfrac{\omega^2 M_{23}^2}{Z_3}} \tag{2}$$

$$Z_{IN,4} = Z_1 + \frac{\omega^2 M_{12}^2}{Z_2 + \dfrac{\omega^2 M_{23}^2}{Z_3 + \frac{\omega^2 M_{34}^2}{Z_4}}} \tag{3}$$

respectively, where Z_{1-4} are the equivalent impedances of an individual coil isolated from all other coils

In order to design an impedance matching network for any of these wireless power configurations, an important consideration is the ratio of the source impedance R_S (typically 50 Ω for a power amplifier) to the real component of the input impedance of the resonator (R_{in}), and *vice versa* for the load side. This impedance ratio R_{in}/R_S determines the quality factor of the matching network. If the impedance ratio is very large (or very small), then the matching network would exceed the minimum (or maximum) quality factor for a designable network [19], [20]. Additionally, for larger ranges of impedance ratios across all coupling coefficients, it is more difficult to
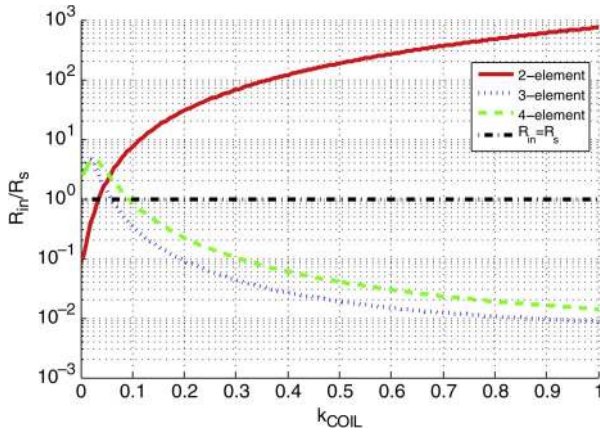
Fig. 7. *Calculated ratio (R_{in}/R_S) of coil to source impedance where $R_{in} = \text{real}(Z_{in})$ and $R_s = 50\ \Omega$ for the calculated input impedance of a two-, three-, and four-coil wireless power system as a function of the coupling coefficient (k_{COIL}) between the two high-Q coils for each configuration.*

physically design an adaptive matching network because more switches will be required to achieve the same tuning capabilities as a set of MCRs with a smaller range of impedance ratios. Therefore, it is desirable to select the coil configuration that achieves the smallest range of impedance ratios across all coil–coil coupling coefficients to ensure maximum power transfer and to simplify the fabrication of an adaptive impedance matching network.

Fig. 7 shows how the impedance ratio R_{in}/R_S changes as a function of the coupling coefficient between the two high-Q coils in each configuration. Recall that the coupling coefficient is related to the mutual inductance by $k_{ij} = M_{ij}/\sqrt{L_iL_j}$. For a two-element system, the impedance ratio is low for weak coupling (k_{12}), and increases by a factor of k_{12}^2 for stronger coupling. For three- and four-element systems, the impedance ratio is high for weak coupling (k_{23}) and decreases by a factor of $1/k_{23}^2$ for stronger coupling. Fig. 7 shows that for this set of MCRs, the four-element system does offer the lowest range of impedance ratios.

C. Using Impedance Matching as a Coil-Tuning Mechanism

To reiterate the importance and practicality of impedance matching, it is useful to refer back to Fig. 4. Panel B shows the input impedance of the blue coils shown in Fig. 3. It is clear that if the system was transmitting at a frequency that did not correspond with the desired load impedance, an impedance matching network could be designed to match the source and the load. However, as Section IV-B showed, the input impedance changes as a function of distance and orientation between the Tx and Rx coils, and thus a dynamically reconfigurable solution is needed. In this section, we will demonstrate how to design an adaptive impedance matching network that can match

the constant source impedance to the varying load impedance for a range of coupling coefficients.

A mismatch between source and load impedances substantially degrades power transfer efficiency at operating frequencies within the narrow ISM band. With a four-element wireless power system, this impedance mismatch has been overcome under narrowband conditions by varying the loop-to-coil coupling coefficients k_{lc} [8], [21]. However, this method of tuning k_{lc} is impractical because it requires mechanically adjusting the distance between the loop and the coil. High-efficiency narrowband operation can also be achieved by using adaptive impedance matching networks to constantly match the varying input impedance of the MCRs to the constant source impedance R_S [20], [22]–[24].

To further understand this concept, we can compare the plots of $|S_{21}|$ as a function of frequency for the blue coils both with and without impedance matching networks. Fig. 4 shows $|S_{21}|$ data for the blue coils (shown in Fig. 3) without the matching networks at a separation distance of 7.8 cm along the common axis of the coils. This plot shows two resonant modes (overcoupled region) and indicates that the efficiency is highest at 12 MHz and is nearly at its lowest at 13.56 MHz. Fig. 8 shows $|S_{21}|$ data for the blue coils with impedance matching networks at both the input to the Tx loop and at the output of the Rx loop. This plot shows that there are four resonant peaks, and the marker indicates that maximum efficiency occurs at the peak corresponding to 13.56 MHz. In this example, efficiency was increased from 24.2% to 75.7% using the matching network. Although maximum efficiency can be achieved for both approaches used in Figs. 4 and 8, Fig. 8 demonstrates that only impedance matching networks
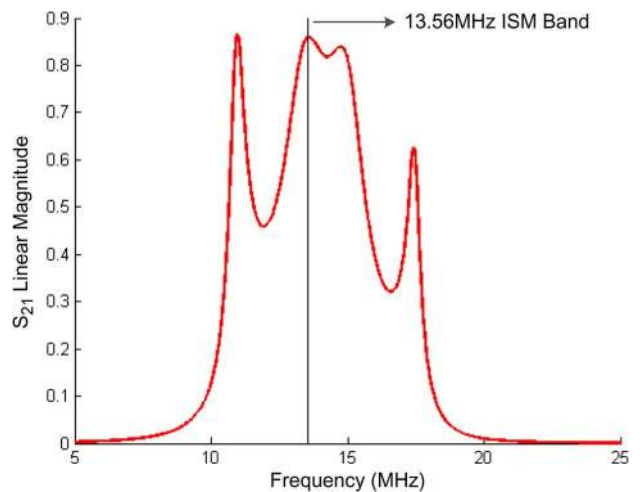
Fig. 8. *Measured $|S_{21}|$ for the blue coils with π-match networks at both Tx and Rx sides at a distance of 7.4 cm along the axis of the coil. Clearly visible are the four resonant modes caused by the coupling of the two high-Q resonators and the impedance matching networks.*
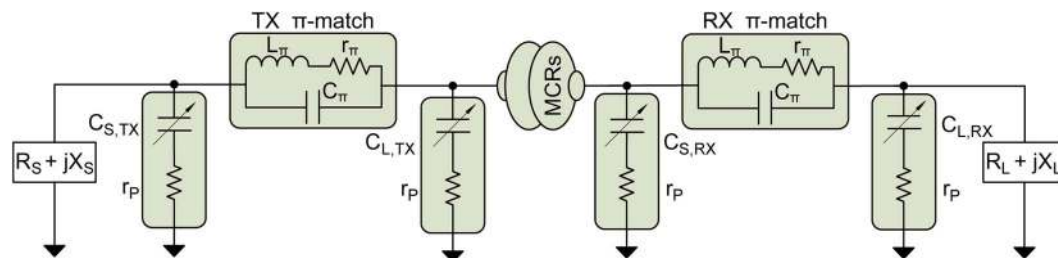
Fig. 9. *Schematic diagram of the dynamic impedance matching technique used at both Tx and Rx sides for a set of MCRs. Each variable capacitor indicated in this figure has been implemented as a bank of four capacitors that can be switched manually (four switches for the Tx π-match and four switches for the Rx π-match).*

can achieve maximum efficiency within the allowable 13.553–13.567-MHz ISM bandwidth.

D. Adaptive Impedance Matching With a π-Match Network

Fig. 9 shows a block diagram of the wireless power system using adjustable π-match networks for dynamic impedance matching. This topology includes variable source capacitors C_S, variable load capacitors C_L, a fixed inductor L_π with parasitic resistance and capacitance (r_π and C_π), and the parasitic equivalent series resistance r_p of the capacitors. The variable source and load capacitances are implemented with a four-element switched capacitor bank.

This circuit can perform impedance matching by dynamically controlling the source and load capacitance of both π-match networks. Compared to other matching network topologies such as the L-match, the π-match is ideal for adaptive wireless power transfer because it uses a fixed-value inductor in the high-current path while variable capacitors handle minimal power in shunt configurations [19], [20], [25]. Additionally, Fig. 7 shows that across a range of coil coupling coefficients, the input impedance to the MCRs can vary from greater than, equal to, or less than the fixed 50-Ω source impedance. The π-match topology can accommodate all of these cases, while an L-match topology can only match in one direction.

Another design consideration is whether to place a matching network at both Tx and Rx sides versus only at a single side. A π-match network at both the input to the Tx loop and the output of the Rx loop can result in a wider range of impedance matching between source and load impedances, thus resulting in higher wireless power transfer efficiency at a single frequency for any separation distance [20].

E. Capacitor Selection Tools for a π-Match Network

A Matlab algorithm has been developed that uses unconstrained nonlinear optimization to determine the ideal capacitor values for a π-match network that will maximize S_{21} for a range of coil–coil coupling coefficients. This algorithm takes measured S-parameters for a given L_π and set of MCRs and converts the S-parameters into ABCD-matrices. The ABCD representation is convenient because a series of cascaded two-port networks can be modeled by computing the product of their individual ABCD matrices to form a single lumped ABCD-matrix. The ABCD matrices for the Tx π-match network, the MCRs, and the Rx π-match network are multiplied together. After converting the lumped ABCD-matrix back to an S-matrix, the source and load capacitor values in each π-match network are determined by selecting values that optimize $|S_{21}|$ at the desired frequency.

A total of 100 data sets were collected from the VNA for incremental distances of 3.7 cm between the blue Tx and Rx coils spanning a 60 × 60-cm^2 *x–y* grid for both parallel and perpendicular configurations, as in panels 1A and 2A of Fig. 6. These data were logged for the blue coils without the π-match networks. Importing these S-parameters into the Matlab simulation allows for the ideal source and load π-match capacitor values to be determined across every distance such that the maximum S_{21} occurs at 13.56 MHz.

Next, two printed circuit boards (PCBs) of the π-match networks are connected to the Tx and Rx blue coils as in Fig. 9. Although it is possible to select the capacitor values using general purpose input/output (GPIO) pins from a microcontroller, this prototype uses DIP switches to manually enable or disable the source and load capacitors of the π-match networks. A full set of data is retaken using a single operating frequency (13.56 Mhz) with a transmit power of 5 W for the same 60 × 60-cm^2 grid in Fig. 6 using the recommended capacitor values from the Matlab simulation. The π-match PCBs are used as the π-match network, and the capacitor values are manually switched to the optimal value for each receive coil position on the grid. Table 1 shows the capacitor values used on the π-match PCBs. These boards use surface-mount ceramic 0603 capacitors, and the inductors used in the π-match networks are 206-nH Coilcraft Maxi-Spring Air Core inductors.

Panels 1D and 2D in Fig. 6 show the measured wireless power transfer efficiency for adaptive impedance

Table 1 Switched Capacitor Bank Values for the π-Match Networks Used for Adaptive Impedance Matching

Component	Switch 1*	Switch 2	Switch 3	Switch 4
$C_{S,TX}$	68 pF	120 pF	270 pF	470 pF
$C_{L,TX}$	9 pF	33 pF	47 pF	68 pF
$C_{S,RX}$	2 pF	15 pF	47 pF	68 pF
$C_{L,RX}$	68 pF	120 pF	270 pF	470 pF
r_p	0.2 Ω	0.2 Ω	0.2 Ω	0.2 Ω

*The switch number refers to the capacitance that can be switched in using the DIP switches. For example, the maximum capacitance that can be used for $C_{S,TX}$ is the parallel combination of all four capacitors (68+120+270+470pF = 928pF).
**The inductor values $L_{\pi,TX}$ and $L_{\pi,RX}$ are fixed at 206nH.

matching. Due to the frequency splitting effect in the overcoupled regime, the wireless power transfer efficiency at a single frequency (Fig. 6, panel 1B) is very low for short separation distances. The adaptive frequency tracking technique (Fig. 6, panel 1C) outlined in Section III achieves high efficiency in the overcoupled regime, but violates FCC regulations by operating outside the 13.56-MHz band and is, therefore, not likely to be used in practical applications. At the origin in Fig. 6, the efficiency at 13.56 MHz is improved from 13% for the case without adaptation (panel 1B) to 89% efficiency using adaptive impedance matching (panel 1D). The efficiency for short separation distances is not quite as high as the efficiency for adaptive frequency tracking because the capacitor values implemented with the π-match PCBs are not able to perfectly match the source and load impedances, and because of the parasitic resistance associated with each switch. For the same reasons listed here, Fig. 5 also shows reduced efficiency for the adaptive impedance matching curve compared to the adaptive frequency tracking curve for regions of strong coupling (small angular misalignments). However, a scrutiny of Fig. 6 shows that adaptive impedance matching achieves a slight improvement in the efficiency at longer distances between the Tx and Rx coils.

To demonstrate adaptivity to variations in angular misalignment, efficiency measurements are retaken for the case when the coils are oriented at 90°. For this worst case alignment, the coupling between the MCRs never reaches the overcoupled region. Therefore, panels 2B and 2C are almost identical because maximum efficiency occurs at a single frequency in the undercoupled region. Panel 2D shows a slight improvement in range using adaptive impedance matching because the matching network is able to match the 50-Ω source impedance to the high load impedance caused by weak coupling between the MCRs, as seen in Fig. 7.

The results from this figure show that it is possible to achieve high efficiency while operating at a single frequency in the overcoupled regime and a slight range extension in the undercoupled regime using adaptive impedance matching.

V. ADAPTIVE RECTIFICATION

Thus far, adaptation techniques have been presented that focus on modifying the operating parameters of the coils themselves, either by changing the input and output impedance of the coils using an RF matching network or by choosing the operating frequency that stimulates one of the resonant modes of the coils. However, these approaches have assumed steady state loading conditions that are not realistic for applications where the end device varies its power consumption as a function of activity. Furthermore, a significant challenge in developing effective wireless power systems is the efficient rectification of RF power to direct current (dc) power across the system's operating points. This issue arises from the need to maintain optimal impedance matching between the receiving antenna and the rectifier while the load impedance of the application changes.

A. System Overview

In order to address these challenges, an adaptive rectifier has been developed which uses a nonlinear impedance matching circuit element and a custom control algorithm to adapt to changes in distance (i.e., coupling coefficient) and fluctuations in the load.

A diagram of the adaptive rectifier is shown in Fig. 10. Starting from the left, RF power from the magnetic coupled resonators (or other sources) is injected into the full-wave rectifier block, which converts the RF power into dc. Next, the adaptive impedance matching circuit, which consists of a microcontroller, voltage and current sensing circuits, and a feedforward buck converter, is used to control the ratio of voltage to current that is drawn off of the rectifier and deliver to the load. Although buck converters are typically used for voltage regulation, they can also be thought of as nonlinear impedance matching circuits for dc systems. Finally, power is delivered to the load application, which for the purpose of this work is represented as a current source. This approximation is made since most electronic devices require a constant supply voltage with varying load current. It should be noted that this work
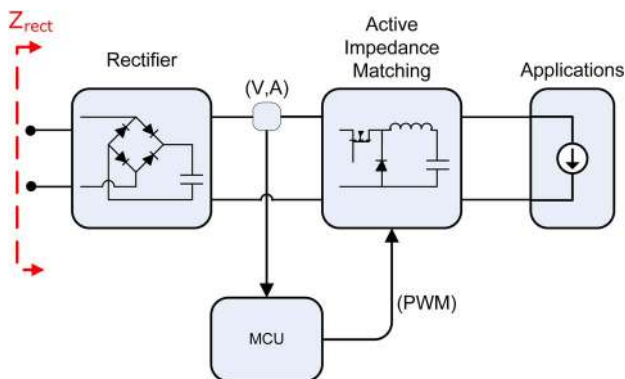
Fig. 10. *Maximum power point tracking method using an active feedforward buck converter and microcontroller to control the input impedance of the enhanced rectifier.*

focuses on improving the efficiency of the rectifier. Additional control algorithms and/or voltage regulation stages may be needed for a particular application.

The system architecture and the control algorithms implemented on the microcontroller are similar to maximum power point tracking (MPPT) techniques used for harvesting the maximum possible power from solar cells [26], [27]. In that application, the optimal I–V ratio of the solar cells is a function of the incident light on the panels. In this work, the output of the MCRs presents a variable source resistance, and a typical application will present a variable load resistance. Thus, adaptation techniques are needed to ensure maximum power transfer.

A prototype of the adaptive rectifier is shown in Fig. 11. It consists of a full bridge rectifier, over-voltage protection,
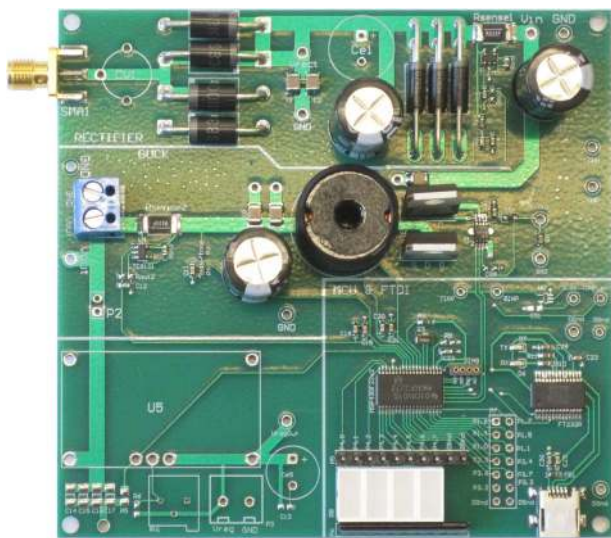
Fig. 11. *Prototype of the adaptive rectifier capable of delivering power at nearly constant efficiency to the load application over a wide range of loading conditions.*

a high-voltage synchronous N-Channel MOSFET driver (LTC4444), circuits for measuring voltage and current, and an MSP430 microcontroller, which is used to implement the control algorithm for tracking the maximum power point of the rectifier. This prototype was designed for robustness and fault tolerance. Further optimization and size reduction are possible for future integration into end devices.
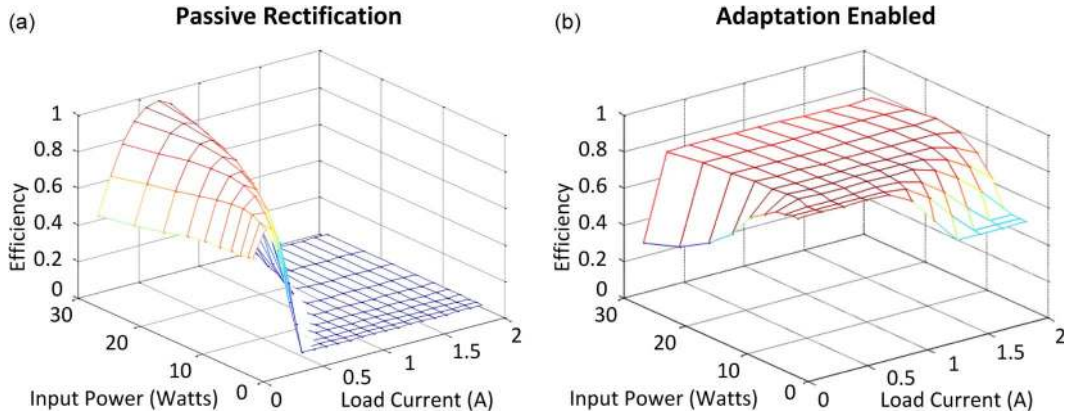
B. Load Matching

One under-appreciated aspect of RF rectifier design is that changes in load impact the impedance match between the RF antenna and the input of the rectifier itself. Occasionally, poor power transfer to the load can be misinterpreted as inefficiencies in the rectifier. In reality, RF power is being reflected off of the rectifier-antenna interface due to loading conditions.

To highlight the issue of load matching and to demonstrate the effectiveness of the new adaptive rectifier, the prototype was tested at various input power levels and loading conditions. In this experiment, a class "A" RF power amplifier (from *AR RF/Microwave Instrumentation*, model 100W1000B) with a source impedance of approximately 50 Ω was connected to the input adaptive rectifier prototype. The RF amplifier swept its output power from 3–30 W at a fixed frequency of 13.56 MHz. At each sweep point, an electronic load (model #: HP 6063B) provided a second sweep of load current, which emulated different power consumption modes that an application might present. The resulting rectified output voltages and currents were recorded using digital multimeters (DMMs). A host computer running Labview was used to control the system and record data. It should be noted that the output impedance of the RF amplifier was measured and found to be stable across these limited output powers and loading conditions.

Fig. 12 shows two sets of plots of system transfer efficiency: one of a normal rectifier (that is, with adaptation turned off) and the other with adaptive impedance matching enabled. In the 3-D plots, the axes are the swept input power versus the swept load current, and the surface represents the efficiency of RF-to-dc rectification at each point. Panel A shows the result when adaptation is turned off. This is the standard case for passive rectifiers powering variable loads. The key takeaway is that if the wrong loading conditions are applied to the rectifier, an impedance mismatch occurs between the output of the coils and the input of the rectifier, and this mismatch results in poor power transfer. Thus, there is only a narrow ridge of points where maximum power transfer can be achieved.

In panel B of Fig. 12, the adaptive impedance matching circuit is enabled. At each data point in the plot (i.e., at each input power and load current), the MSP430 microcontroller measures the output voltage and current ratio being delivered to the load. Its control algorithm adjusts the pulse width modulation signal driving the feedforward

Fig. 12. *Wireless power transfer efficiency as a function of input power and load current as received by the adaptive impedance matching rectifier. Panel A shows the behavior of the system without adaptive matching. Panel B shows the result of enabling the adaptive rectifier which allows for constant efficiency at nearly any input power level and load current.*

buck converter and uses a gradient–ascent method to maximize rectified power. The result is that for nearly any input power level and load current, an operating point can be found that maximizes power transfer. This is shown as a plateau of near-constant transfer efficiency. The result is that rectifiers that use MPPT techniques can effectively mitigate load variation, which would normally disrupt power transfer.

C. Adaptive Impedance Matching

Section V-B described a method for controlling the apparent load impedance seen by the output of the rectifier so that the maximum amount of RF power could be harvested. In effect, the loading condition on the rectifier maintained the optimal impedance match between the input of the rectifier and the output of the RF source. The other way to look at the system is that if the source im-

pedance of the MCRs was not 50 Ω, the maximum power point tracking algorithm on the microcontroller will still servo the PWM control signal to maximize the power transfer. This will in turn change the real component of the input impedance to the rectifier to closely match the output impedance of the amplifier.

To demonstrate this property of the adaptive rectifier, it was analyzed by a custom-built 100-W vector network analyzer (VNA). The results can be seen in Fig. 13. Here the VNA transmits a single tone of 13.56 MHz at 12.5 W into the adaptive rectifier prototype. Then, the duty cycle of the buck converter was varied from 20% to 80%. The resulting impedances are shown on the Smith chart in panel A. Note that the trace on the Smith chart is not frequency, but rather the duty cycle of the PWM signal controlling the feedforward buck converter element. The magnitude of the input impedance $|Z_{11}|$ versus duty cycle is shown in panel B.
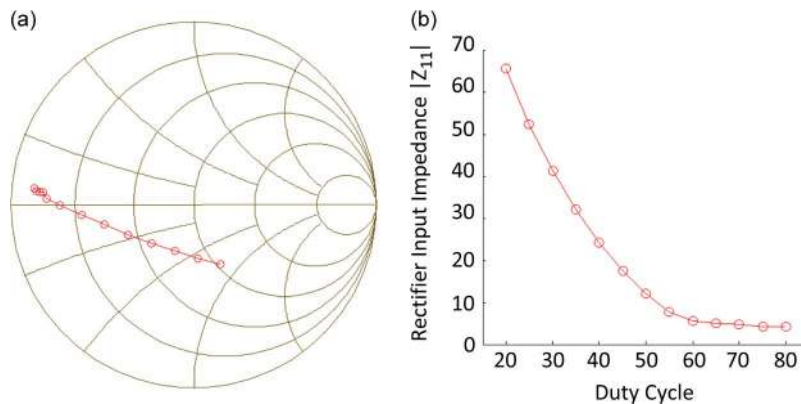
Fig. 13. *Input impedance of the adaptive rectifier when the duty cycle of the nonlinear impedance matching block is varied from 20% to 80%. Panel A depicts a Smith chart of the input impedance which shows a mostly real dependency on duty cycle. Panel B shows the magnitude of the input impedance $|Z_{11}|$ versus duty cycle.*
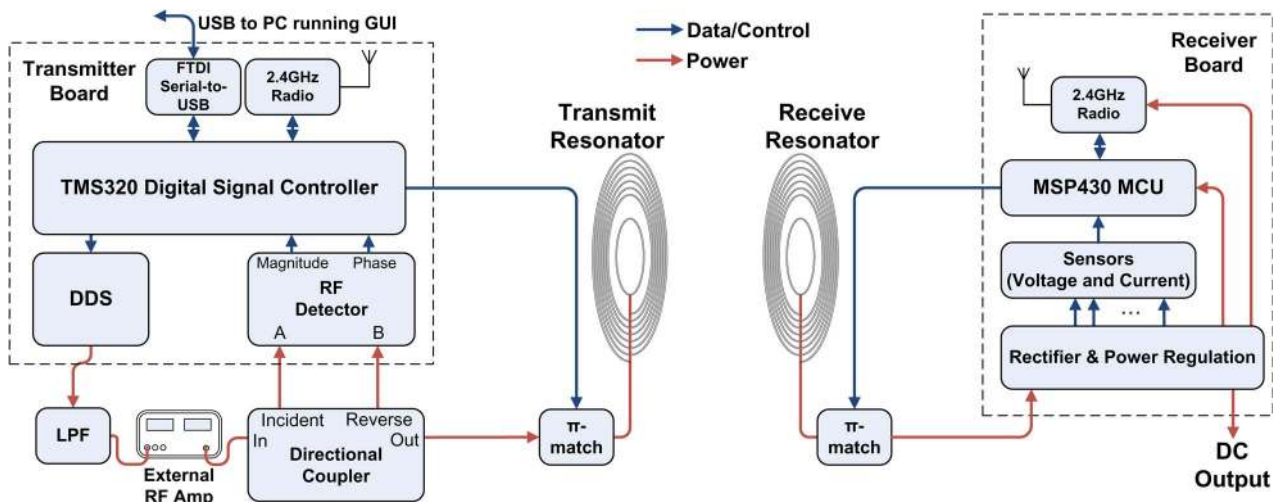
Fig. 14. *Block diagram of the end-to-end wireless power system. Power is denoted with red lines, while data and/or control is denoted with blue lines. In the case of the TMS320's connection to the DDS, the blue connection denotes a digital control word. In the case of the DSC's connections to the USB controller and 2.4-GHz radio, the blue lines represent serial digital data. On the receive board, blue lines indicate the measurements of multiple voltage and current sensors, which may be used to send information back to the transmitter via its 2.4-GHz radio about the state of its operating conditions. Finally, the blue lines going to the π-match boards indicate GPIO control pins controlling capacitor banks.*

The two panels show that controlling the duty cycle of the feedforward buck converter allows the adaptive rectifier to servo its input impedance. The range of this prototype is between 5 and 65 Ω. However, the Smith chart shows that some reactance is introduced, and the impedance matching is not purely real. This is believed to be due to the junction capacitance of the diodes. One solution could be to mitigate this parasitic reactance with a switched impedance matching network. Ultimately, this shows that using a feedforward buck converter to form an adaptive rectifier is an effective means of electronically controlling the RF impedance of a rectifier using only solid-state devices.

VI. APPLICATION

Using these ideas, a practical end-to-end system can be built that seamlessly delivers wireless power to the full volume of space available. The ideas of dynamic frequency tuning and impedance matching inform the system requirements. For dynamic frequency tuning, the transmitter should be able to change its output frequency on the fly, provide amplification, and detect how much power is being delivered to the load. Dynamic impedance matching requires the transmitter to control impedance-matching circuits, such as the π-match boards mentioned in Section IV. To track moving loads that rapidly change system operating conditions, the smart transmitter should be able to respond quickly to transient events. The main types of events include human-caused changes in position and orientation, as well as variations in the load's power demands.

A. System Description

With these principles and guidelines in mind, a working prototype of a full end-to-end system has been developed. A block diagram of the complete system is shown in Fig. 14. The implementation of a smart transmitter is shown in the left panel of Fig. 15, and the RF receiver and power management unit is shown in the right panel of Fig. 15.

The heart of the transmitter module consists of a Texas Instruments TMS320 digital signal controller (DSC), a microcontroller that includes some DSP functionality. The DSC controls all peripherals on the board and communicates with an external personal computer (PC) via a serial-to-USB FTDI chip. The external PC runs a graphical user interface that can be used to easily set various parameters of the system.
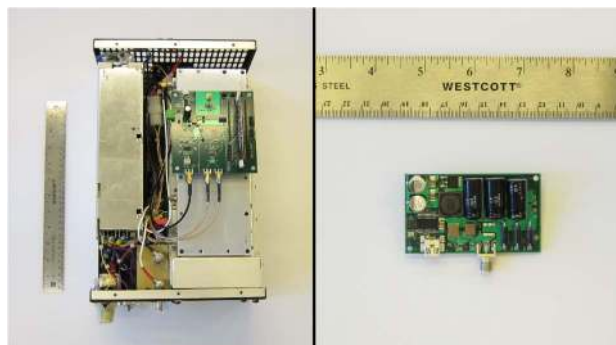
Fig. 15. *Images of the transmitter board with external amplifier (left) and the receiver board (right).*

To detect the phase and magnitude of the RF signal being transmitted to the load, a high-power directional coupler is used to extract the incident and reflected signals, which are then routed to inputs of an Analog Devices AD8302 RF detector integrated circuit (IC). The RF detector outputs two voltages that are proportional to the log magnitude ratio and phase between the incident and reflected power (i.e., $1/S_{11}$). Since the DSC is clocked at 150 MHz, it may take many digital samples of this voltage in a short period of time. In fact, it takes this system only 5 μs to take one data point.

Using these measurements of the forward and reflected waveform, the DSC adjusts the transmit frequency of the systems via an Analog Devices AD9850, an RF direct digital synthesizer (DDS). Since the DDS produces a sampled sinusoid from a reference clock, higher order harmonics need to be filtered out to produce a clean signal. This is done with an off-the-shelf low-pass filter with a cutoff of 22 MHz.

Additionally, the transmitter can also employ dynamic impedance matching by controlling π-match boards via parallel GPIO interfaces from the DSC. An external RF amplifier is used to achieve an output power of up to 100 W.

The receiver unit rectifies the RF power from the coils and delivers regulated power to the load application. An MSP430 microcontroller from Texas Instruments uses voltage and current sensing circuits to monitor system performance and aids in startup procedures. Both the transmitter and the receiver include 2.45-GHz Texas Instruments CC2500 radios, which implement out-of-band communication. This bidirectional communication allows the DSC and host application to receive streaming data on the load power consumption and enables the transmitter and host application to send commands to the receiver unit. Future iterations of the receiver board will include an adaptive rectification controller and battery recharging functionality.

B. System Operation and Control Algorithms

The system's control algorithm has two goals: choose the optimal system parameters (transmit frequency or π-match settings) given the current system state, and maximize power transfer over time. Different considerations must be made for frequency tuning and impedance matching.

1) Dynamic Frequency Tuning: In this case, the transmitter changes its transmit frequency to maximize power transfer by tracking one of the resonant modes. Other systems, such as [28] and [29], have used similar approaches by measuring estimates of the total reflected power at different discrete frequencies. These systems also modify either the increments between the discrete frequencies or the number of frequency points measured to find a more optimal transmit frequency. In [30], a dif-
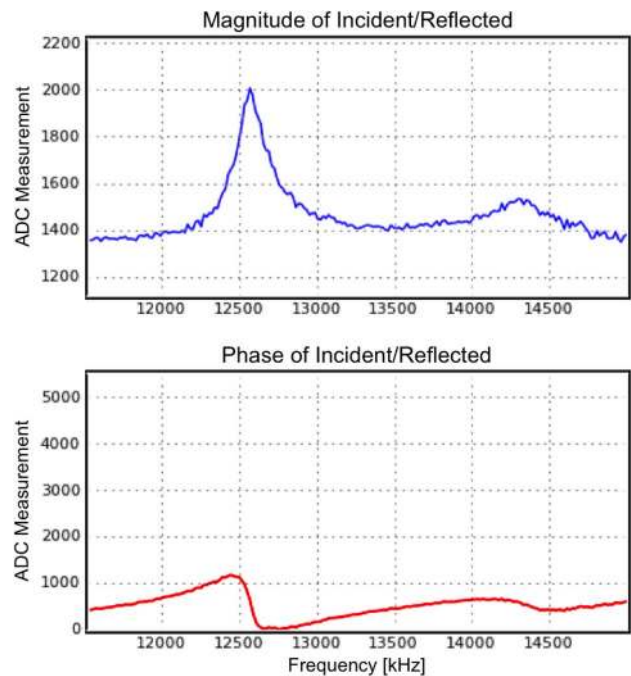
Fig. 16. *Typical spectrum of the overcoupled regime measured by our system.*

ferent, analog method of frequency tuning is used. Though we use a somewhat similar method of control as [28] and [29], our system is optimized for different requirements: to seamlessly power moving objects in a volume of space. As such, we use a somewhat different algorithm that adaptively narrows or widens the frequency increment between a small number of frequency points as required.

A naive implementation of frequency tuning would sweep N frequency points across the entire spectrum of use, measuring $|1/S_{11}|$ at each one. Once the sweep is taken, the point with maximum $|1/S_{11}|$ is chosen as the new transmit frequency. Fig. 16 shows a typical frequency sweep performed by the system.

To maximize power delivery over time, the system can take advantage of the peaked shape of the spectrum and perform gradient ascent. This requires the system to only measure a few points on each iteration. Such an algorithm can be further improved by progressively decreasing the frequency increments as the system hones in on an optimal operating point. This procedure is similar to the approach used by [28], with the main difference being that our system does not start with the same frequency increment at the beginning of each sweep. Rather, our system only changes the frequency increment for a sweep when it detects that the load or environmental conditions have changed.

The algorithm operates as follows: after an initial optimal transmit frequency is chosen using a full sweep, m points are examined on either side of the current

operating point. This means only $N = 2m + 1$ points are measured on each iteration (a good value is $N = 5$ or $N = 7$). The points are spaced in frequency steps of Δf. After these N points are sampled and stored in memory, the frequency which corresponds to the maximum $|1/S_{11}|$ is chosen as the new operating point. The algorithm also updates the frequency step on iteration i as follows:

- if the center point is chosen on iteration i, $\Delta f_{i+1} = (1/2) \cdot \Delta f_i$;
- if an edge point is chosen, $\Delta f_{i+1} = 2 \cdot \Delta f_i$;
- if any other point is chosen, $\Delta f_{i+1} = \Delta f_i$.

This adaptive algorithm allows the bandwidth of the transmitted signal to progressively narrow, maximizing the wireless power transfer efficiency, because less time is spend off of the resonant peak. At the same time, any changes in the spectrum caused by perturbations in load position or orientation cause the system to temporarily widen its bandwidth to seek out the new optimal transmit frequency. These operations happen very quickly (with $N = 5$ and $\Delta t_s = 5 \, \mu s$, one sweep occurs in 25 μs), which allows the system to track high-speed loads [moving at up to (1 cm/25 μs) = 400 (m/s)].

2) Impedance Matching: The system is also capable of fixed frequency operation by using dynamic impedance matching. π-match boards have been built that contain capacitor banks that can be switched on or off by a parallel GPIO interface. The search space for π-match is more complicated than that of frequency tuning. Where frequency tuning's search space was 1-D, the space for impedance matching is 2-D, as the system can change both the Tx-side or Rx-side capacitances. The search space ends up having $2^{(n_{Tx}+n_{Rx})}$ states, where n_{Tx} and n_{Rx} are the number of capacitors on the Tx and Rx sides, respectively. Thus, the bank capacitor values must be chosen carefully to provide the most effective matching circuit with the fewest number of capacitors. However, some control values will not correspond to optimal impedance matches, and may be excluded from the search space ahead of time.

Unfortunately, the π-match space does not have smooth peaks that correspond to optimal operating points, so gradient ascent cannot be used. This means that a sweep and peak-hold algorithm is the best option. Detection of delivered power presents another challenge to using impedance matching. The $|1/S_{11}|$ measurement used for frequency tuning tends to be somewhat unreliable with π-match. Thus, a measurement of the throughput power is more effective. However, this means that the load needs to send information back to the transmitter. This is accomplished by communicating information about received power back from the load using the out-of-band radio.

C. System Demonstration

A video demonstrating the prototype's performance may be found in this work's supporting materials. To provide an idea of how seamlessly the system can adapt to a nonstationary load, the system wirelessly powers a moving lightbulb using adaptive frequency tuning. In the first part of the video, the system only uses a single transmit frequency. In this case, the lightbulb only illuminates at a specific distance. In the next part of the video, we turn on adaptive frequency tuning. Now the lightbulb always remains on, regardless of how quickly the position or orientation of the receiving coil changes. This is because the system quickly adjusts the operating frequency to maintain optimal efficiency.

We have also experimented with powering useful consumer and biomedical applications with our system. These devices include a laptop, a cellphone, and a left ventricular assist device (LVAD) [31]. See Fig. 17 for an image of a wirelessly powered cellphone. By attaching a receiver board that contains a small loop and coil, a rectifier, and a regulator, our solution can provide power to the cellphone
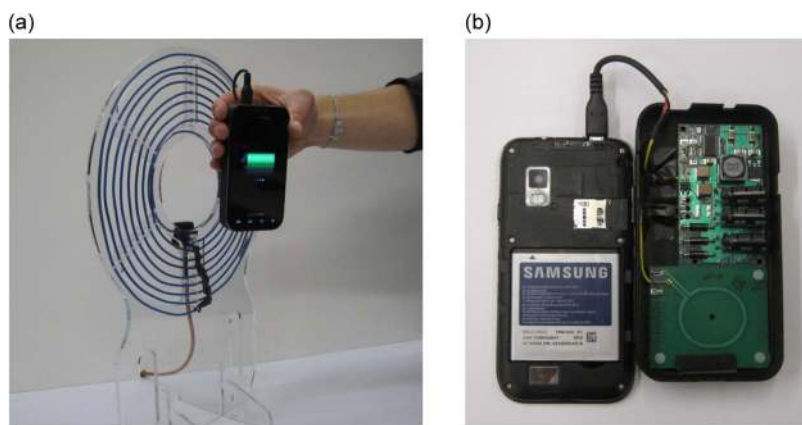
Fig. 17. *Wirelessly powered cellphone. Panel A shows the phone being powered by a large transmit coil within a region of 10 cm. Panel B shows the small receive loop and coil, rectifier, and regulator attached to the USB charging port of the cellphone.*

anywhere around the coil. Using dynamic frequency tuning from 8 to 22 MHz, the system can seamlessly adapt to changes in distance and orientation between the transmitter and the cellphone.

VII. CONCLUSION

In this paper, we argue that wireless power systems based on MCRs can realize the vision of seamless, reliable wireless power delivery if they are able to adapt to variations in range, orientation, and loading conditions. The key insight is that the over-coupled regime allows for high efficiency and near-constant power delivery if the system is tuned properly.

In particular, we have demonstrated that adaptive impedance matching techniques used for fixed frequency operation and adaptive frequency tuning for wider bandwidth systems can enable wireless power delivery to larger areas of space than previously published work. Additionally, we have introduced an adaptive rectifier topology that is capable of adapting to changes in loading conditions to allow optimal power delivery. Conversely, the adaptive rectification technique also allows a receiver to control its input impedance to ensure proper matching to the MCRs. Finally, we present a full end-to-end system capable of adapting to real-time changes in the environment while maintaining optimum efficiency. ∎

Table 2 Measured Lumped Element Values for Each of the Individual Circuit Elements for the Experimental Blue Coils

TRANSMITTER		RECEIVER	
L_1	0.6708uH	L_4	0.6737uH
C_1	203.19pF	C_4	203.6pF
R_{p1}	0.2627Ω	R_{p4}	0.2586 Ω
N_1	1	N_4	1
$Radius_1$	10.25cm	$Radius_4$	10.25cm
R_{source}	50 Ω	R_{load}	50 Ω
Q_1	1.143	Q_4	1.145
F_1	13.63MHz	F_4	13.58MHz
K_{12}	0.2798	K_{34}	0.287
Q_2	312.9	Q_3	230.29
F_{o2}	13.68MHz	F_{o3}	13.66MHz
L_2	17.04uH	L_3	17.15uH
C_2	8pF	C_3	8pF
R_{p2}	4.66 Ω	R_{p3}	6.36 Ω
N_2	8	N_3	8
$Radius_2$	14cm	$Radius_3$	14cm

APPENDIX

Table 2 shows a summary of all the extracted parameters for both loops and coils shown in Fig. 3. All of these parameters were extracted using the model outlined in [8].

REFERENCES

[1] PowerMat Technologies, Nov. 2011. [Online]. Available: www.powermat.com

[2] S. Ahson and M. Ilyas, *RFID Handbook: Applications, Technology, Security, Privacy.* Boca Raton, FL, USA: CRC Press, 2008.

[3] A. Sample and J. Smith, "Experimental results with two wireless power transfer systems," in *Proc. IEEE Radio Wireless Symp.*, Jan. 2009, pp. 16–18.

[4] W. Brown, "The history of power transmission by radio waves," *IEEE Trans. Microw. Theory Tech.*, vol. MTT-32, no. 9, pp. 1230–1242, Sep. 1984.

[5] J. McSpadden and J. Mankins, "Space solar power programs and microwave wireless power transmission technology," *IEEE Microw. Mag.*, vol. 3, no. 4, pp. 46–57, Dec. 2002.

[6] U.S. Federal Communications Commission (FCC), *Title 47: Telecommunication, Part 15 Radio Frequency Devices*, Jan. 31, 2011. [Online]. Available: www.fcc.gov

[7] A. Kurs, A. Karalis, R. Moffatt, J. D. Joannopoulos, P. Fisher, and M. Soljacic. (2007). Wireless power transfer via strongly coupled magnetic resonances. *Science* [Online]. *317(5834)*, pp. 83–86. Available: http://www.sciencemag.org/cgi/content/abstract/317/5834/83

[8] A. Sample, D. Meyer, and J. Smith, "Analysis, experimental results, range adaptation of magnetically coupled resonators for wireless power transfer," *IEEE Trans. Ind. Electron.*, vol. 58, no. 2, pp. 544–554, Feb. 2011.

[9] B. Cannon, J. Hoburg, D. Stancil, and S. Goldstein, "Magnetic resonant coupling as a potential means for wireless power

transfer to multiple small receivers," *IEEE Trans. Power Electron.*, vol. 24, no. 7, pp. 1819–1825, Jul. 2009.

[10] Z. N. Low, R. Chinga, R. Tseng, and J. Lin, "Design and test of a high-power high-efficiency loosely coupled planar wireless power transfer system," *IEEE Trans. Ind. Electron.*, vol. 56, no. 5, pp. 1801–1812, May 2009.

[11] J. Casanova, Z. N. Low, and J. Lin, "A loosely coupled planar wireless power system for multiple receivers," *IEEE Trans. Ind. Electron.*, vol. 56, no. 8, pp. 3060–3068, Aug. 2009.

[12] T. Imura, "Study on maximum air-gap and efficiency of magnetic resonant coupling for wireless power transfer using equivalent circuit," in *Proc. IEEE Int. Symp. Ind. Electron.*, Jul. 2010, pp. 3664–3669.

[13] A. Christ, M. G. Douglas, J. M. Roman, E. B. Cooper, A. P. Sample, B. H. Waters, J. R. Smith, and N. Kuster, "Evaluation of wireless resonant power transfer systems with human electromagnetic exposure limits," *IEEE Trans. Electromagn. Compat.*, doi: 10.1109/TEMC.2012.2219870. [Online]. Available: http://ieeexplore.ieee.org/stamp/stamp.jsp?tp=&arnumber=6340322&isnumber=4358749

[14] N. Fletcher and T. Rossing, *The Physics of Musical Instruments.* New York, NY, USA: Springer-Verlag, 1998.

[15] U. S. Federal Communications Commission (FCC), *Title 47: Telecommunication, Part 18 Radio Frequency Devices*, Jan. 31, 2011. [Online]. Available: www.fcc.gov

[16] M. Kiani, U.-M. Jow, and M. Ghovanloo, "Design and optimization of a 3-coil inductive link for efficient wireless power

transmission," *IEEE Trans. Biomed. Circuits Syst.*, vol. 5, no. 6, pp. 579–591, Dec. 2011.

[17] M. Kiani and M. Ghovanloo, "The circuit theory behind coupled-mode magnetic resonance-based wireless power transmission," *IEEE Trans. Circuits Syst. I, Reg. Papers*, vol. 59, no. 9, pp. 2065–2074, Sep. 2012.

[18] A. RamRakhyani, S. Mirabbasi, and M. Chiao, "Design and optimization of resonance-based efficient wireless power delivery systems for biomedical implants," *IEEE Trans. Biomed. Circuits Syst.*, vol. 5, no. 1, pp. 48–63, Feb. 2011.

[19] Y. Sun and J. Fidler, "Design method for impedance matching networks," *Inst. Electr. Eng. Proc.—Circuits Devices Syst.*, vol. 143, no. 4, pp. 186–194, Aug. 1996.

[20] S. A. P. Waters, B. H. Smith, and J. R. Smith, "Adaptive impedance matching for magnetically coupled resonators," in *Proc. Progr. Electromagn. Res. Symp.*, Aug. 2012, vol. 2, no. 1, pp. 694–701.

[21] T. P. Duong and J.-W. Lee, "Experimental results of high-efficiency resonant coupling wireless power transfer using a variable coupling method," *IEEE Microw. Wireless Compon. Lett.*, vol. 21, no. 8, pp. 442–444, Aug. 2011.

[22] T. Beh, M. Kato, T. Imura, S. OH, and Y. Hori, "Automated impedance matching system for robust wireless power transfer via magnetic resonance coupling," *IEEE Trans. Ind. Electron.*, 2012, DOI: 10.1109/TIE.2012.2206337.

[23] T. Beh, M. Kato, T. Imura, and Y. Hori, "Wireless power transfer system via magnetic resonant coupling at fixed resonance frequency—Power transfer

system based on impedance matching," in *Proc. 25th Symp. Exhibit. World Battery Hybrid Fuel Cell Electr. Veh.*, Nov. 2010, vol. 4, pp. 744–753.

[24] J. Park, Y. Tak, Y. Kim, Y. Kim, and S. Nam, "Investigation of adaptive matching methods for near-field wireless power transfer," *IEEE Trans. Antennas Propag.*, vol. 59, no. 5, pp. 1769–1773, May 2011.

[25] M. Thompson and J. Fidler, "Determination of the impedance matching domain of impedance matching networks," *IEEE Trans. Circuits Syst. I, Reg. Papers*, vol. 51, no. 10, pp. 2098–2106, Oct. 2004.

[26] A. N. A. Ali, M. H. Saied, M. Z. Mostafa, and T. M. Abdel-Moneim, "A survey of maximum

PPT techniques of PV systems," in *Proc. IEEE Energytech*, May 2012, DOI: 10.1109/EnergyTech.2012.6304652.

[27] T. Paing, J. Shin, R. Zane, and Z. Popovic, "Resistor emulation approach to low-power RF energy harvesting," *IEEE Trans. Power Electron.*, vol. 23, no. 3, pp. 1494–1501, May 2008.

[28] T. Deyle and M. Reynolds, "Powerpack: A wireless power distribution system for wearable devices," in *Proc. 12th IEEE Int. Symp. Wearable Comput.*, Oct. 1, 2008, pp. 91–98.

[29] N. Kim, K. Kim, J. Choi, and C.-W. Kim, "Adaptive frequency with power-level tracking system for efficient magnetic

resonance wireless power transfer," *Electron. Lett.*, vol. 48, no. 8, pp. 452–454, 2012.

[30] P. Si, A. Hu, S. Malpas, and D. Budgett, "A frequency control method for regulating wireless power to implantable devices," *IEEE Trans. Biomed. Circuits Syst.*, vol. 2, no. 1, pp. 22–29, Mar. 2008.

[31] B. H. Waters, A. P. Sample, P. Bonde, and J. R. Smith, "Powering a ventricular assist device (VAD) with the free-range resonant electrical energy delivery (FREE-D) system," *Proc. IEEE*, vol. 100, no. 1, pp. 138–149, Jan. 2012.

ABOUT THE AUTHORS

Alanson P. Sample (Member, IEEE) received the B.S., M.S., and Ph.D. degrees in electrical engineering from the University of Washington (UW), Seattle, WA, USA, in 2005, 2008, and 2011, respectively.

Currently, he is a Research Scientist at Intel Labs, Hillsboro, OR, USA, working on power autonomous sensing and computing devices, energy harvesting, and wireless power delivery. At the time that this research was conducted, he was a Postdoctoral Research Associate at the Computer Science and Engineering Department, UW, and a Lecturer in Electrical Engineering at UW Bothell. Throughout his graduate studies, he worked at Intel Labs, Seattle, WA, USA, as both a full time employee and as an intern. During his time at Intel, he published several articles on the use of magnetically coupled resonators for wireless power delivery, as well as papers on radio-frequency identification (RFID) and ambient radio-frequency (RF) energy harvesting. He was one of the key contributors to the Wireless Identification and Sensing Platform, which was open-sourced in 2009 as part of Intel's WISP Challenge. His research interests lie broadly in the area of wireless power including: antenna theory and design, energy harvesting from ambient and deliberate sources, novel sensing and computing elements, and the application of these systems.

Benjamin H. Waters (Student Member, IEEE) received the B.A. degree in physics from Occidental College, Los Angeles, CA, USA, in 2010 and the B.S. degree in electrical engineering from Columbia University, New York, NY, USA, in 2010, as part of the 3-2 Combined Plan. He is currently working toward the Ph.D. degree in electrical engineering at the University of Washington, Seattle, WA, USA.

As an undergraduate, he worked in the Columbia Integrated Systems Laboratory (CISL), Columbia University, where he completed research on wireless power transfer. He has several internship experiences with Network Appliance, Arup, and most recently with Intel Labs Seattle in 2010, where he continued his research in wireless power transfer. His research interests lie mostly in the field of wireless power, including near-field antenna design, adaptive maximum power point tracking systems, and applications for these systems including biomedical, military, and consumer electronics.

Mr. Waters is a member of Tau Beta Pi and Pi Mu Epsilon.

Scott T. Wisdom (Student Member, IEEE) received the B.S. degree in electrical and computer engineering and the B.A. degree in English from the University of Colorado Boulder, Boulder, CO, USA, in 2010. He is currently working toward the Ph.D. degree in electrical engineering at the University of Washington, Seattle, WA, USA.

He has worked as a full-time R&D Engineer at Fluke Networks, Everett, WA, USA, where he worked on a variety of embedded hardware and software for test and measurement of copper and wireless networks. His research interests include statistical signal processing and machine learning, as well as embedded and wireless systems.

Joshua R. Smith (Senior Member, IEEE) received the B.A. degree in computer science and philosophy from Williams College, Williamstown, MA, USA, in 1991, the M.A. degree in physics from Cambridge University, Cambridge, U.K., in 1997, and the Ph.D. and S.M. degrees from the MIT Media Lab, Cambridge, MA, USA, in 1999.

He is an Associate Professor of Electrical Engineering and of Computer Science and Engineering at the University of Washington, Seattle, WA, USA, where he leads the Sensor Systems research group. From 2004 to 2010, he was Principal Engineer at Intel Labs, Seattle, WA, USA. He is interested in all aspects of sensor systems, including creating novel sensor systems, powering them wirelessly, and using them in applications such as robotics, ubiquitous computing, and human–computer interaction. At Intel, he founded and led the Wireless Resonant Energy Link (WREL) project, as well as the Wireless Identification and Sensing Platform (WISP) project, and the Personal Robotics project. Previously, he coinvented an electric field sensing system for suppressing unsafe airbag firing that is included in every Honda car. He is the editor of a book entitled *Wirelessly Powered Sensor Systems and Computational RFID* (New York, NY, USA: Springer–Verlag, 2013).